An Evaluation of Adaptive Biomechanical Non-Rigid Registration for Brain Glioma Resection Using Image-Guided Neurosurgery

Fotis Drakopoulos, Chengjun Yao, Yixun Liu, and Nikos Chrisochoides

1 Introduction

Malignant gliomas are the most common primary brain tumors, accounting for approximately 70% of the 22,500 new cases of primary brain tumors annually diagnosed in adults in the USA [1]. The heterogeneity and infiltrative nature of gliomas suggests that a resection within or adjacent to the eloquent areas is challenging and carries a risk of post-operative neurologic deficit [2]. Therefore, the main challenge for neurosurgeons in glioma surgery is to achieve a maximal tumor resection while still preserving eloquent areas.

Image-guided neurosurgery (IGNS) has yielded faster, safer, and more effective minimally invasive procedures [3–8]. During the procedure (i.e., after the opening of the skull and dura), the shape of the brain changes because of the cerebrospinal fluid drainage, gravity, the application of dehydrolyzing agent, and other operations (i.e., resection, retraction), introducing discrepancies in relation to the pre-operative configuration. Interventional MRI can compensate for the intra-operative brain deformation. However, the acquisition of other image modalities (fMRI, DT-MRI) is impractical due to long processing time (e.g., a 3T MAGNETOM Verio scanner requires about 20 min to acquire a DT-MRI and more than 30 min to acquire a BOLD fMRI).

Commonly, commercial systems exclusively use rigid registration to project the pre-operatively acquired imaging (MRI, fMRI, and DT-MRI) into the navigational system; however, a number of studies have tracked surface points in the brain

F. Drakopoulos • Y. Liu • N. Chrisochoides (✉)
The Department of Computer Science, Old Dominion University, Norfolk, VA, USA
e-mail: npchris@gmail.com

C. Yao
The Department of Neurosurgery, Huashan Hospital, Shanghai, China

A. Wittek et al. (eds.), *Computational Biomechanics for Medicine*,
DOI 10.1007/978-3-319-54481-6_10

and reported that movements on the order of a centimeter or more can occur intra-operatively [9]. Additionally, shift can occur in deep subcortical white matter because of tissue retraction, lateral ventricle, and the application of a dehydrolyzing agent. Therefore, a non-rigid registration is necessary to accurately capture the soft tissue deformation induced by tumor resection.

A commonly used non-rigid transformation model is based on the finite element method (FEM). FE biomechanical models allow more principled control of localized deformations and have been applied to improve the efficacy and efficiency of brain surgery [3–8, 10–13]. An FE model is represented by a series of Partial Differential Equations (PDEs), which describe the physical deformation of the underlying tissues. The tissues are delineated in the image by using a segmentation technique [14, 15]. The segmented image is tessellated into a volumetric mesh and each element is assigned to a local physical description of the anatomical structure to which it belongs. To find the numerical solution of the PDEs, constraints are applied to the model, and a linear system of equations is solved to compute the displacements on the mesh vertices. A dense deformation field can be estimated by interpolating the computed mesh displacements at each image voxel.

Meshless methods have been presented as alternatives to FE methods. A Meshless Total Lagrangian Explicit Dynamics (MTLED) algorithm was developed to compute soft tissue deformation in surgical simulation [16]. This method was accurate in terms of overall reaction forces but not quite as good with individual displacements or forces. In [17] a MTLED-based suite of algorithms was used to perform a comprehensive patient-specific surgical simulation. The results obtained using MTLED were as useful and accurate as those obtained with the FE method.

The produced non-rigid transformation can be useful to create augmented reality visualizations of pre-operative multi-modal imaging (MRI, fMRI, DT-MRI) with iMRI, and thus to facilitate real-time resection guidance in glioma surgery involving language areas and neighboring subcortical motor pathways (e.g., Pyramid Tracts). Figure 1a depicts such a visualization. The DTI tractography is shown in real-time together with a tumor model (red) during the neurosurgical resection.

The augmented reality visualization helps neurosurgeon to achieve an appropriate volumetric resection while preserving neighboring subcortical motor pathways.

The aim of this paper is to evaluate the efficiency (i.e., accuracy, robustness) of two adaptive biomechanical non-rigid registration methods [3, 4] to compensate for the brain deformation induced by cerebral glioma resection. The first method employs a point/element outlier rejection scheme integrated into a Nested Expectation and Maximization framework to simultaneously resolve the point correspondence, the deformation field, and the resection region. The second approach iteratively estimates a dense deformation field by inclemently and accurately incorporating small changes in the geometry of the domain resulted by tumor resection. The evaluation performed on MRI data from ten patients who underwent partial, complete, and extended glioma resection at Huashan Hospital. Structural MRI (SPGR, MP-RAGE, FLAIR, T2w) were acquired prior and during each surgery

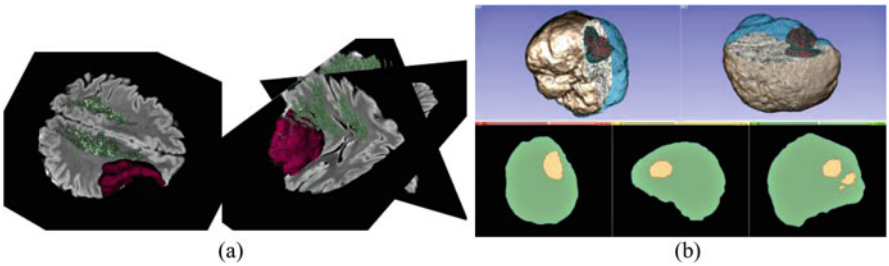

Fig. 1 (**a**) Non-rigid alignment of pre-operative DTI tractography with iMRI. The fused image shows that the partially resected tumor is directly adjacent to the Pyramid Tracts. (**b**) Multi-tissue mesh (number of tetrahedra: 160,179; minimum dihedral angle: 4.41°). Top row: mesh superimposed on MRI. *Cyan* and *red* represent the surface of the brain parenchyma mesh and the tumor mesh, respectively. Bottom row: mesh fidelity illustrated on an axial, sagittal, and coronal slice. Each slice depicts an intersection between the mesh surface (*cyan and red lines*) and the segmented volume (*green and yellow regions*). The closer the mesh surface to the physical image boundaries, the higher the mesh fidelity

with a 3T movable scanner. The registration accuracy was assessed on totally 40 volumetric alignments by: (i) a visual inspection, (ii) a Hausdorff Distance (HD)-based error metric, and (iii) a landmark-based error measured by neurosurgeon.

2 Materials and Methods

2.1 Patient Population

Ten patients with an age range of 19–75 years underwent surgery on a single, unilateral, and supratentorial primary glioma from September 2010 to August 2013. The lesions involved in Pyramid Tracts (PTs) were in cortical regions in the motor or somatosensory areas, cortical regions adjacent to the central gyrus, subcortical regions with an infiltrative progression along the PTs, and/or deep temporal or insular regions in relation to the internal capsule. Pre- and intra-operative brain images were obtained in the integrated neurosurgical suite (IMRIS, Winnipeg, Manitoba, Canada) using a ceiling-mounted movable 3.0 T MAGNETOM Verio scanner (Siemens AG, Erlangen, Germany) with a 70 cm working aperture. A neurosurgeon categorized the image data as: (i) Partial Tumor Resection (PTR), (ii) Complete Tumor Resection (CTR), and (iii) Extensive Tumor Resection (ETR). Table 1 lists the clinical data.

Table 1 Clinical MRI data

			Image Size (voxels)		Image Spacing (mm)	
#	Genre	Type	Pre-op	Intra-op	Pre-op	Intra-op
1	M	PTR	448 × 512 × 176	512 × 448 × 176	0.488 × 0.488 × 1	0.488 × 0.488 × 1
2	M	PTR	448 × 512 × 80	512 × 456 × 66	0.468 × 0.468 × 2	0.468 × 0.468 × 2
3	M	PTR	448 × 512 × 176	512 × 448 × 176	0.488 × 0.488 × 1	0.488 × 0.488 × 1
4	M	CTR	512 × 448 × 176	512 × 448 × 176	0.488 × 0.488 × 1	0.488 × 0.488 × 1
5	F	CTR	448 × 512 × 176	448 × 512 × 176	0.488 × 0.488 × 1	0.488 × 0.488 × 1
6	M	CTR	448 × 512 × 176	384 × 512 × 144	0.488 × 0.488 × 1	0.488 × 0.488 × 1
7	M	ETR	448 × 512 × 144	448 × 512 × 144	0.488 × 0.488 × 1	0.488 × 0.488 × 1
8	F	ETR	512 × 456 × 66	456 × 512 × 66	0.468 × 0.468 × 2	0.468 × 0.468 × 2
9	F	ETR	512 × 456 × 66	512 × 456 × 68	0.468 × 0.468 × 2	0.468 × 0.468 × 2
10	M	ETR	448 × 512 × 176	448 × 512 × 176	0.488 × 0.488 × 1	0.488 × 0.488 × 1

PTR partial tumor resection, *CTR* complete tumor resection, *ETR* extensive tumor resection

2.2 Segmentation

The biomechanical non-rigid registration in this study requires a pre-operative segmentation. Pre-operative imaging is usually acquired few days before the first intra-operative acquisition, therefore any computational requirements of a pre-operative segmentation are easily satisfied. Before the segmentation, the brain is extracted from the skull using the BET tool [14]. Then a combination of automatic operators implemented in 3D Slicer (i.e., region growing and level-set filters) [15] and a slice-by-slice manual segmentation is performed to correct any erroneously included regions. An evaluation on how the segmentation accuracy affects the registration accuracy is beyond the scope of this paper, however, it will be included in our future work.

2.3 Rigid Registration

The first intra-operative scan is acquired after the head of the patient is positioned for the craniotomy and fixed but before the opening of the skull. At this stage no brain shift occurs. A Rigid Registration (RR) was performed with the BRAINSFit module in 3D Slicer v4.4.0 [18] to compensate for any translations or rotations between the pre- and the intra-operative image. RR uses a Versor Rigid 3D Transform (VR3DT) to apply a rotation and translation to the space. RR relies on histogram bins and spatial samples to estimate a Mattes Mutual Information (MMI) cost metric for the alignment. The larger the number of samples, the slower and more precise the fit. In order to achieve higher accuracy, we set 100 histogram levels and 5% sampling percentage (50 and 0.2% are the default values, respectively). For the rest of the RR parameters we used the default values.

2.4 Adaptive Non-Rigid Registration

The last 10 years we explored the feasibility of three biomechanical non-rigid registration methods to compensate for the brain deformation induced by tumor resection: (i) A Physics-Based Non-Rigid Registration (PBNRR) integrated on ITK and 3D Slicer [19]; (ii) A Nested Expectation-Maximization Non-Rigid Registration (NEMNRR) [3, 20]; (iii) An Adaptive Physics-Based Non-Rigid Registration (APBNRR) [4, 21]. NEMNRR, and APBNRR are adaptive; PBNRR is non-adaptive.

The above non-rigid registration methods do not simulate the skull or an interaction between the brain parenchyma and the skull. Before the registration, the pre-operative and the intra-operative intracranial brain cavities are extracted from the skull [14]. A sparse displacement field is computed from the distances between features in the pre-operative intracranial cavity and their corresponding features in the intra-operative intracranial cavity. PBNRR and APBNRR rely on a cross correlation metric to compute the corresponding features. NEMNRR relies on a Gaussian distribution function. A tetrahedral mesh of the brain parenchyma is generated from a segmented pre-operative intracranial cavity and the sparse displacement field is applied on the mesh nodes. The prescribed displacement field implicitly accounts for a brain–skull interaction in the case where corresponding features are located on the surface of the brain parenchyma. In this study, the nodes on the parenchyma surface are free to translate in three-dimensions as no explicit interaction between the brain and the skull is assumed.

A linear assumption is used for the displacements and the materials of the model. The values of the mechanical properties of the isotropic materials (i.e., Young's modulus, Poisson ratio) were obtained from [8]. These values were extrapolated from best-fit data obtained in porcine studies. For tumor, a value ten times stiffer than that for normal tissue is used (Table 2). The adaptive methods employ a heterogeneous model (brain parenchyma, tumor). The non-adaptive method employs a homogeneous model (brain parenchyma). The quality of the tetrahedral mesh (e.g., dihedral angle) influences the accuracy of the numerical solution of a linear system of equations and thus, the correctness of the estimated transformation. The higher the quality of the elements (e.g., the larger the minimum dihedral angle), the better the conditioning of the coefficient matrix and, consequently, the convergence of the linear solver. Figure 1b depicts a multi-tissue mesh used for biomechanical non-rigid registration. Parameter δ (Table 2) determines the size of the mesh ($\delta > 0$).

NEMNRR formulates the registration as a three-variable (point correspondence, deformation field, and resection region) functional minimization problem, in which point correspondence is represented by a fuzzy assign matrix, deformation field is represented by a piecewise linear function regularized by the strain energy of a heterogeneous biomechanical model, and resection region is represented by a maximal connected tetrahedral mesh. This method utilizes a point/element outlier rejection incorporated into a Nested Expectation and Maximization framework to simultaneously resolve these three variables. Figure 2 illustrates the NEMNRR framework.

Table 2 Parameters for non-rigid registration

Parameter	Value	Description	Method
Connectivity pattern	face	Pattern for block selection	PBNRR, APBNRR
F_s	5%	% selected blocks from total number of blocks	PBNRR, APBNRR
$B_{s,x} \times B_{s,y} \times B_{s,z}$	$3 \times 3 \times 3$	Block size (in voxels)	PBNRR, APBNRR
$W_{s,x} \times W_{s,y} \times W_{s,z}$	$9 \times 9 \times 3$ (PTR), $13 \times 13 \times 3$ (CTR, ETR)	Block matching window size (PBNRR, APBNRR) or Search range (NEMNRR) (voxels).	All
R	0.93	Annealing factor	NEMNRR
δ	5	Mesh size	All
E_b , ν_b	2.1 KPA, 0.45	Young's modulus, Poisson ratio for brain parenchyma	All
E_t , ν_t	21 KPA, 0.45	Young's modulus, Poisson ratio for tumor	NEMNRR, APBNRR
F_r	25%	% of rejected outlier blocks	PBNRR, APBNRR
N_{rej}	10	Number of outlier rejection steps	PBNRR, APBNRR
$N_{iter,.max}$	10	Max number of iterations	APBNRR
$N_{b0,min}$	1% of the total number of blocks	Minimum number of blocks without a correspondence	APBNRR

All: PBNRR, NEMNRR, APBNRR

APBNRR iteratively estimates a dense deformation field by inclemently and accurately incorporating small changes in the geometry of the domain resulted by tumor resection. The computation of the dense field is facilitated by a sparse displacement vector associated with highly discriminant blocks inside the cranial cavity, and a heterogeneous biomechanical model which describes the physical deformation of the brain. After each deformation, the quality of the elements deteriorates, and thus the model is globally re-meshed in real-time using a Delaunay meshing algorithm [22] to avoid the heavily distorted elements, and to recover the anatomical boundaries with geometric guarantees. Figure 3 illustrates the APBNRR framework. The model is globally re-meshed from a warped segmented image to capture not only the brain deformations but also the complex geometric changes nearby the tumor margins, while maintaining throughout the process meshes with good quality elements—critical for the accuracy and convergence rate of the solver.

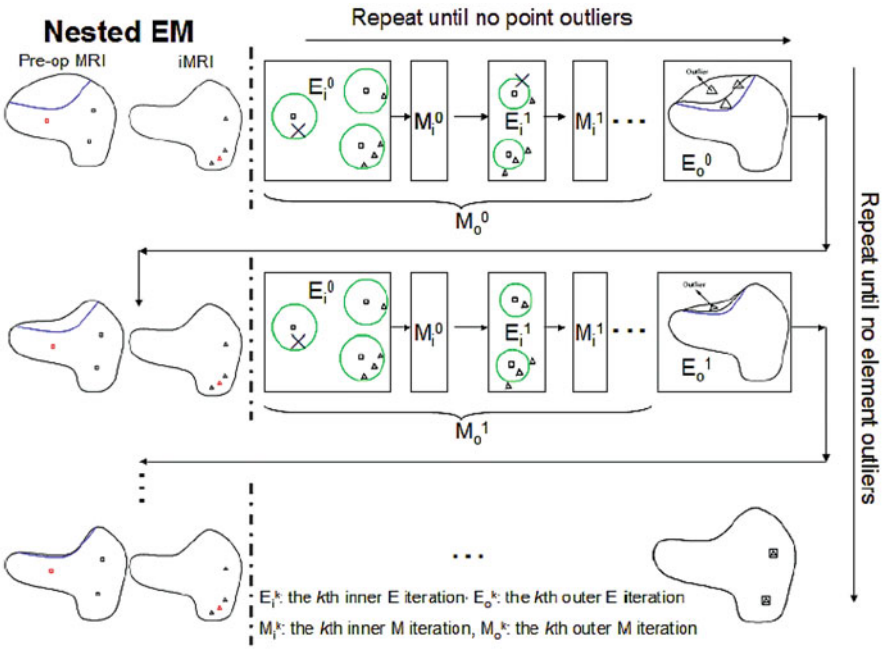

Fig. 2 Nested Expectation Maximization framework [3]. In the horizontal direction, the inner EM iteratively estimates the correspondence and the deformation field until no point outliers are detected. In the vertical direction the outer EM rejects the element outliers and computes the resected region

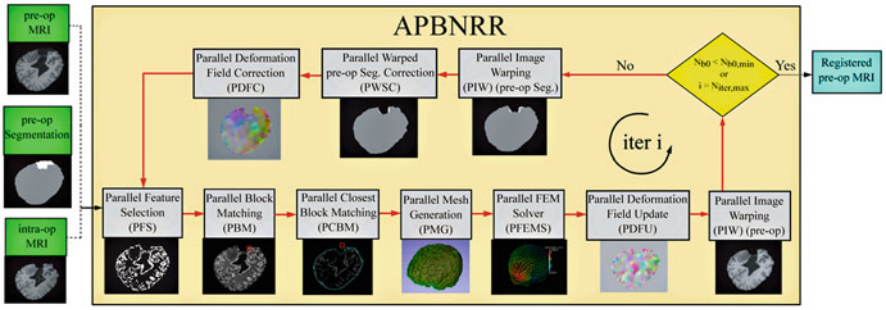

Fig. 3 APBNRR framework [4]. The red arrows show the execution order of the different modules in the loop. The loop breaks when the number of blocks without correspondence is less than a threshold or when the maximum number of iterations has been reached

3 Results

We performed an evaluation on imaging data from ten patients underwent partial, complete, and extended glioma resection. We assessed the registration accuracy with a visual inspection, a Hausdorff Distance (HD)-based error metric, and a landmark-based error measured by a neurosurgeon. Table 2 presents the parameters used for the non-rigid registration. More details about the parameters of each method are given in [3, 4, 19].

3.1 Visual Assessment

In most applications, careful visual inspection remains the first and most important validation check available for previously unseen data. Figure 4 depicts a qualitative assessment for six patients of this study. For each patient, we depict an intra-operative MRI, a registered pre-operative MRI, and a subtraction between the intra-operative and the registered pre-operative MRI. Based on Fig. 4, APBNRR aligns more accurately the MR images and preserves the brain morphology during the neurosurgical resection, especially near the tumor margins. The assessment shows that the quality of the alignments is not significantly affected by the volumetric resection (partial, complete, or extended). In contrast, the other methods show significant misalignments near the tumor cavities.

3.2 Quantitative Assessment with the HD Metric

We employed a publicly available implementation of the Hausdorff Distance (HD) metric [23] to quantitatively evaluate the registration accuracy. This metric is a measurement of the degree of mismatch between two point sets. The first set is extracted from the pre-operative volume, and then it is transformed according to the estimated deformation field. The second point set is extracted from the intra-operative volume. The HD metric is computed between the transformed point set and the fixed point set. For the point extraction, we employed a Canny edge detection implemented in ITK. Compare to a previous evaluation of the registration accuracy [5], this study uses the 100% HD metric. The smaller the HD value, the more precise the alignment ($HD \geq 0$). The ideal case with perfect alignment is when HD is equal to 0. The ratio $= HD_X/HD_Y$ denotes how many times more accurate one method is when compared to another. When ratio > 1 then method Y is ratio times more accurate than method X. Table 3 presents the results. We computed a total of 40 HD errors. APBNRR achieved the smallest error in each individual case, and the smallest average error (3.69 mm) among all the methods. APBNRR is on average, 6.83, 6.41, and 6.34 times more accurate compared to RR, PBNRR, and NEMNRR, respectively.

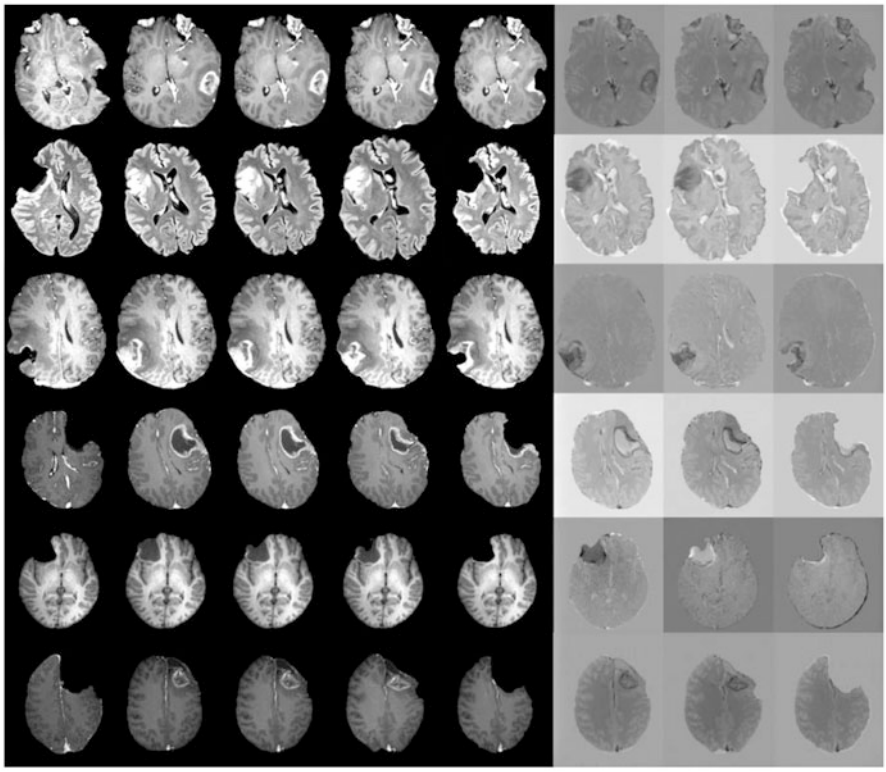

Fig. 4 Qualitative evaluation of the registration accuracy. *Each row* represents a single case. We depict the same representative slice for all the images belonging to the same row. The results were confirmed by a neurosurgeon who inspected the full registered volumes. From top to bottom row: PTR cases 1, 2; CTR cases: 4, 5; ETR cases: 7, 9. From left to right column: (**a**) intra-op MRI; (**b**) RR pre-op MRI; (**c**) PBNRR pre-op MRI; (**d**) NEMNRR pre-op MRI; (**e**): APBNRR pre-op MRI; (**f**): (**a**) subtracted from (**c**); (**g**): (**a**) subtracted from (**d**); (**h**): (**a**) subtracted from (**e**)

3.3 Quantitative Assessment with Anatomical Landmarks

A neurosurgeon quantitatively evaluated the alignment accuracy on six anatomical locations, as suggested in [24]. The neurosurgeon selected six landmarks in the pre-operative volume and identified their correspondent locations in the intra-operative volume. Two landmarks were selected at the cortex near the tumor depending on the shift of the brain surface; other two landmarks were selected at the anterior horn and at the triangular part of the lateral ventricle; the last two landmarks were selected at the junction between the pons and mid-brain and at the roof of fourth ventricle. For each landmark, the error was calculated as the distance between the physical location of the point in the intra-operative volume and its transformed location in

Table 3 Quantitative evaluation of the registration accuracy with a HD metric

Case	Type	HD_{RR}	HD_{PBNRR}	HD_{NEMNRR}	HD_{APBNRR}	$\frac{HD_{RR}}{HD_{APBNRR}}$	$\frac{HD_{PBNRR}}{HD_{APBNRR}}$	$\frac{HD_{NEMNRR}}{HD_{APBNRR}}$
1	PTR	16.15	15.12	15.08	4.60	3.51	3.29	3.28
2	PTR	26.89	26.89	23.87	4.00	6.72	6.72	5.97
3	PTR	29.93	27.76	28.11	2.83	10.58	9.81	9.93
4	CTR	17.90	15.56	16.84	4.11	4.36	3.79	4.10
5	CTR	30.37	28.96	28.96	3.13	9.70	9.25	9.25
6	CTR	23.22	21.44	21.27	3.08	7.54	6.96	6.91
7	ETR	17.59	16.63	15.20	4.19	4.20	3.97	3.63
8	ETR	32.32	30.13	30.20	3.45	9.37	8.73	8.75
9	ETR	18.48	18.15	17.86	3.97	4.65	4.57	4.50
10	ETR	27.07	24.91	25.16	3.54	7.65	7.04	7.11
Average		*23.99*	*22.56*	*22.26*	*3.69*	*6.83*	*6.41*	*6.34*

HD_{RR}, HD_{PBNRR}, HD_{NEMNRR}, and HD_{APBNRR} are the alignment error after an RR, PBNRR, NEMNRR, and APBNRR registration, respectively
PTR partial tumor resection, *CTR* complete tumor resection, *ETR* extensive tumor resection. All errors are in mm

Table 4 Quantitative evaluation of the registration accuracy with six anatomical landmarks identified by a neurosurgeon

Method	Average min error	Average max error	Average mean error
RR	3.49	11.96	7.27
PBNRR	1.72	9.94	5.38
NEMNRR	2.31	11.76	6.01
APBNRR	1.52	9.05	4.71

The values are the average minimum, maximum, and mean errors computed on the six anatomical locations, from ten patients. All errors are in mm

the registered volume. For each patient, we calculated a minimum, a maximum, and a mean error based on six landmarks. We then calculated their corresponding average errors for ten patients. Table 4 presents the results. The landmark-based assessment confirms that the APBNRR provides the most accurate alignments on the specific anatomical locations. APBNRR exhibits the lowest average mean error (4.71 mm) which may be clinically useful.

4 Conclusion

A retrospective study was carried out on volumetric MRI data acquired from ten patients. The patients underwent an incomplete, complete, and extensive glioma resection at Huashan Hospital. The accuracy of the alignments was assessed with a: (i) robust HD metric, (ii) anatomical points identified by a neurosurgeon, and (iii) visual assessment inspected by a neurosurgeon.

The experimental evaluation confirmed that a geometric-based adaptive deformable registration approach exhibits the most accurate alignments among all the methods in this study, independently of the volumetric resection (PTR, CTR, or ETR). This method significantly reduces the error due to rigid registration commonly used by commercial neuronavigators within the time constraints imposed by neurosurgery. Indeed, it completes a volumetric alignment, on the average, in 137.90 s (including I/O) on a Linux workstation with 12 Intel Xeon X5690@3.47 GHz CPU cores and 96 GB of RAM.

We observed differences between the alignment errors measured with a Hausdorff Distance metric and manually identified anatomical landmarks. We believe that, this is because the HD approach computes the degree of mismatch between two point sets A , B by measuring the distance of the point of A that is farthest from any point of B and vice versa, but there is no explicit pairing of points of A with points of B [25]. On the other hand, the landmark-based approach measures the Euclidian distance between two but corresponding points, though in some applications (e.g., inter-subject brain registration) the true point-to-point correspondence can never be known and may not even exist.

Acknowledgments Research reported in this publication was supported in part by the Modeling and Simulation Fellowship at Old Dominion University, CCF-1439079, John Simon Guggenheim Foundation, and by the Richard T. Cheng Endowment.

References

1. Louis David N, Hiroko O, Wiestler Otmar D, Cavenee Webster K, Burger Peter C, Anne J, Scheithauer Bernd W, Paul K (2007) The 2007 WHO classification of tumors of the central nervous system. J Acta Neuropathol 114(2):97–109
2. Evren Keles G, Chang EF, Lamborn KR, Tihan T, Chang C-J, Chang SM, Berger MS (2006) Volumetric extent of resection and residual contrast enhancement on initial surgery as predictors of outcome in adult patients with hemispheric anaplastic astrocytoma. J Neurosurg 105(1):34–40
3. Yixun L, Chengjun Y, Fotis D, Wu J, Liangfu Z, Nikos C (2014) A nonrigid registration method for correcting brain deformation induced by tumor resection. Med Phys 41(101710)
4. Drakopoulos F, Chrisochoides NP (2015) Accurate and fast deformable medical image registration for brain tumor resection using image-guided neurosurgery. Comput Methods Biomech Biomed Eng Imaging Visual 4(2):112–126
5. Archip N, Clatz O, Whalen S, Kacher D, Fedorov A, Kot A, Chrisochoides N, Jolesz F, Golby A, Black PM, Warfield SK (2007) Non-rigid alignment of pre-operative MRI, fMRI, and DT-MRI with intra-operative MRI for enhanced visualization and navigation in image-guided neurosurgery. NeuroImage 35(2):609–624
6. Clatz O, Delingette H, Talos IF, Golby A, Kikinis R, Jolesz F, Ayache N, Warfield S (2005) Robust non-rigid registration to capture brain shift from intraoperative mri. IEEE Trans Med Imaging 24(11):1417–1427
7. Michael MI (2015) Computational modeling for enhancing soft tissue image guided surgery: an application in neurosurgery. Ann Biomed Eng 44(1):1–11
8. Miga MI, Roberts DW, Kennedy FE, Platenik LA, Hartov A, Lunn KE et al (2001) Modeling of retraction and resection for intraoperative updating of images. Neurosurgery 49:75–84

9. Dorward NL, Olaf A, Velani B, Gerritsen FA, Harkness WFJ, Kitchen ND, Thomas DGT (1998) Postimaging brain distortion: magnitude, correlates, and impact on neuronavigation. J Neurosurg 88:656–662
10. Mostayed A, Garlapati R, Joldes G, Wittek A, Roy A, Kikinis R, Warfield S, Miller K (2013) Biomechanical model as a registration tool for image-guided neurosurgery: evaluation against bspline registration. Ann Biomed Eng 41(11):2409–2425
11. Wittek A, Miller K, Kikinis R, Warfield SK (2007) Patient-specific model of brain deformation: application to medical image registration. J Biomech 40(4):919–929
12. Ferrant M, Nabavi A, Macq B, Black PM, Jolesz FA, Kikinis R, Warfield SK (2002) Serial registration of intraoperative MR images of the brain. Med Image Anal 6(4):337–359
13. Ferrant M, Nabavi A, Macq B, Jolesz FA, Kikinis R, Warfield SK (2001) Registration of 3-d intraoperative MR images of the brain using a finite-element biomechanical model. IEEE Trans Med Imaging 20(12):1384–1397
14. Smith SM (2002) Fast robust automated brain extraction. Hum Brain Mapp 17(3):143–155
15. Antiga L, Piccinelli M, Botti L, Ene-Iordache B, Remuzzi A, Steinman D (2008) An image-based modeling framework for patient-specific computational hemodynamics. Med Biol Eng Comput 46(11):1097–1112
16. Horton A, Wittek A, Joldes GR, Miller K (2010) A meshless Total Lagrangian explicit dynamics algorithm for surgical simulation. Int J Num Methods Biomed Eng 26(8):977–998
17. Miller K, Horton A, Joldes GR, Wittek A (2012) Beyond finite elements: a comprehensive, patient-specific neurosurgical simulation utilizing a meshless method. J Biomech 45(15):2698–2270
18. Johnson H, Harris G, Williams K. 2007. Brainsfit: mutual information registrations of whole-brain 3d images, using the insight toolkit.
19. Liu Y, Kot A, Drakopoulos F, Yao C, Fedorov A, Enquobahrie A, Clatz O, Chrisochoides NP (2014) An itk implementation of a physics-based non-rigid registration method for brain deformation in image-guided neurosurgery. Front Neuroinfo 8:33
20. Yixun L, Chrisochoides N (2013) Heterogeneous biomechanical model on correcting brain deformation induced by tumor resection. In: Computational biomechanics for medicine. Springer, New York, pp 115–126
21. Drakopoulos F, Liu Y, Foteinos P, Chrisochoides NP (2014) Towards a real time multi-tissue adaptive physics based non-rigid registration framework for brain tumor resection. Front Neuroinfo 8:11
22. Foteinos P, Chrisochoides N (2014) High quality real-time image-to-mesh conversion for finite element simulations. J Parallel Distrib Comput 74(2):2123–2140
23. Commandeur F, Velut J, Acosta O (2011) A VTK algorithm for the computation of the Hausdorff distance. VTK J 839
24. Hastreiter P, Rezk-Salama C, Soza G, Bauer M, Greiner G, Fahlbusch R, Ganslandt O, Nimsky C (2004) Strategies for brain shift evaluation. Med Image Anal 8(4):447–464
25. Huttenlocher DP, Klanderman GA, Rucklidge WJ (1993) Comparing images using the hausdorff distance. IEEE Trans Pattern Anal Mach Intell 15(9):850–863